bioRxiv preprint doi: https://doi.org/10.1101/2025.11.26.690690; this version posted November 30, 2025. The copyright holder for this preprint (which was not certified by peer review) is the author/funder, who has granted bioRxiv a license to display the preprint in perpetuity. It is made available under aCC-BY-NC 4.0 International license.

Epitope and functional classification of human neutralizing antibodies against SFTSV Gn

Qianran Wang[1#], Hao Li[2#], Fanchong Jian[3], Aoxiang Han[2], Yuanni Liu[4], Jingyi Liu[1,5], Yuanling Yu[1], Jing Wang[1], Lingling Yu[1], Yanxia Wang[1], Haiyan Sun[1], Miaomiao Ma[1], Fei Shao[1], Liuluan Zhu[6]*, Wei Liu[2]*, Yunlong Cao[1,3,7]*

[1]Changping Laboratory, Beijing, P.R. China.

[2]State Key Laboratory of Pathogen and Biosecurity, Academy of Military Medical Sciences, Beijing, P.R. China.

[3]Biomedical Pioneering Innovation Center (BIOPIC), School of Life Sciences, Peking University, Beijing, China.

[4]Department of Infectious Diseases, Yantai Qishan Hospital, Yantai, P.R. China.

[5]College of Future Technology, Peking University, Beijing, P. R. China.

[6]Beijing Key Laboratory of Viral Infectious Diseases, Beijing Ditan Hospital, Capital Medical University, Beijing, P.R. China.

[7]Peking-Tsinghua Center for Life Sciences, Peking University, Beijing, P.R. China.

[#]These authors contributed equally.

*Correspondence: yunlongcao@pku.edu.cn (Y.C.), liuwei@bmi.ac.cn (W.L.), zhuliuluan@ccmu.edu.cn (L.Z.)

bioRxiv preprint doi: https://doi.org/10.1101/2025.11.26.690690; this version posted November 30, 2025. The copyright holder for this preprint (which was not certified by peer review) is the author/funder, who has granted bioRxiv a license to display the preprint in perpetuity. It is made available under aCC-BY-NC 4.0 International license.

Abstract

Severe fever with thrombocytopenia syndrome virus (SFTSV) is a lethal bunyavirus lacking approved countermeasures. From SFTS survivors, we isolated 98 human mAbs against the viral glycoproteins Gn and Gc. Gn-specific mAbs showed superior neutralization breadth and potency. Using a high-throughput yeast display deep mutational scanning (DMS) platform, we classified Gn-head mAbs into eight epitope groups, with four groups (IA, ID, IIIA, IIIB) conferring neutralization. Notably, mAbs BD70-4003 (group IA) and BD70-4017 (group IIIA) demonstrated broad neutralization and provided 100% protection in a lethal mouse model. Cryo-EM structural analysis of these mAbs in complex with Gn-head revealed their binding interfaces, which directly validated the epitope residues identified by DMS. Our study delineates the Gn antigenic landscape, identifies potent therapeutic candidates, and establishes DMS coupled with structural validation as a powerful framework for bunyavirus antibody discovery.

Introduction

Severe fever with thrombocytopenia syndrome virus (SFTSV), *Bandavirus dabieense*, is an emerging tick-borne phlebovirus first identified in China in 2009 and now reported across East and Southeast Asia, including Japan, South Korea, Vietnam, Pakistan, and Thailand.[1, 2, 3] Clinical manifestations range from fever, thrombocytopenia, and leukopenia to multi-organ dysfunction, with a subset of patients developing hemorrhagic symptoms and organ failure. Case fatality rates can exceed 30% in some hospital case.[4, 5] The principal vector, the Asian longhorned tick, has also been detected in North America, Russia, and Australia, raising concerns over further geographic expansion, and human-to-human trassmission risk increasing.[6, 7, 8] Despite its designation by the World Health Organization as a priority pathogen requiring urgent countermeasures, no licensed vaccines or effective antiviral drugs are currently available.

The tripartite SFTSV genome encodes a glycoprotein precursor on the M segment, which is cleaved into Gn and Gc that mediate receptor binding and membrane fusion during viral entry.[9, 10] Recent structural studies have resolved key features of these glycoproteins and identified candidate neutralizing epitopes, establishing them as central targets for antibody- and vaccine-based interventions.[11] Several monoclonal antibodies (mAbs) against Gn have been described, but their

bioRxiv preprint doi: https://doi.org/10.1101/2025.11.26.690690; this version posted November 30, 2025. The copyright holder for this preprint (which was not certified by peer review) is the author/funder, who has granted bioRxiv a license to display the preprint in perpetuity. It is made available under aCC-BY-NC 4.0 International license.

efficacy remains insufficient. For example, MAb4-5 neutralizes infection *in vitro* but provides limited protection *in vivo*,[12] Ab10 confers only partial efficacy in animal models,[13] and the broadly neutralizing S2A5 protects against SFTSV in mice but has been tested against a restricted set of strains,[14] 40C10 obtained from mice was reported to identify a new neutralizing epitope in the SFTSV-Gn, however, its affinity is only at the nanomolar (nM) scale.[15, 16] Recently, JK-2, JK-8 and SD4 mAbs isolated from humans showed significant prophylactic and therapeutic efficacy in murine models,[17, 18] suggesting human-derived mAbs with potent neutralization efficacies represent a rational approach to target druggable epitopes on the surface of the SFTSV Gn. Given the identification of these antibodies with varying neutralization efficacy, a systematic and parallel evaluation is essential to delineate the precise relationship between their epitopes and neutralization potency, both *in vitro* and *in vivo*, thereby providing critical insights for developing SFTSV therapeutic antibodies.

Deep mutational scanning (DMS) technology can be employed for epitope distribution and escape mutation analyses at a much higher efficiency than traditional epitope binning techniques.[19, 20] Previously, we presented a high-throughput epitope mapping technology based on DMS to study SARS-CoV-2.[21, 22, 23, 24] By using this technology, an efficient pipeline can be built to isolate a large panel of mAbs and, at the same time, identify their binding epitopes.[25, 26] Similarly, we applied this technology to SFTSV, aiming to elucidate the intrinsic relationship between antigenic epitopes and their functional roles.

Here, we report the isolation and epitope classification of human mAbs from SFTSV-infected convalescents by DMS. We assessed their binding and neutralization using enzyme-linked immunosorbent assay (ELISA) and pseudovirus/authentic neutralization assays, respectively. Using a novel yeast DMS approach for bunyaviruses, we classified the mAbs against Gn-head into eight epitope groups (IA-ID, IIA-IIB, IIIA-IIIB). Four groups (IA, ID, IIIA and IIIB) showed neutralizing activity, with two antibodies—BD70-4003 (IA) and BD70-4017 (IIIA)—exhibiting broad neutralizing activity and providing 100% protection in mice, making them valuable drug candidates. Cryo-electron microscopy (cryo-EM) structural analyses of three mAbs (BD70-4003, BD70-4008 and BD70-4017) defined the molecular basis of antibody recognition and verified the accuracy and reliability of our DMS system applied to the bunyavirus. Our results elucidate the overall epitope distribution of SFTSV Gn-head domain and identify two highly potent neutralizing antibodies

bioRxiv preprint doi: https://doi.org/10.1101/2025.11.26.690690; this version posted November 30, 2025. The copyright holder for this preprint (which was not certified by peer review) is the author/funder, who has granted bioRxiv a license to display the preprint in perpetuity. It is made available under aCC-BY-NC 4.0 International license.

belonging to different epitope groups, which could provide new theoretical guidance for antibody therapeutics and vaccine design.

Results

Isolation of mAbs from SFTS convalescents.

We collected whole-blood samples from 12 SFTSV-infected convalescents, all of whom had been infected for more than one year (Supplementary Table 1). Serum samples were isolated for detection of viral Gn/Gc-specific IgG titers and neutralizing activities against SFTSV pseudovirus were detected. The results showed that Gn or Gc reactive antibody remained at high levels in these serum samples (Fig. 1A), and each exhibited neutralizing activity against six pseudovirus strains (Fig. 1B). This is consistent with previous reports that SFTSV glycoproteins induce long-lasting antibodies, and also suggests the possibility of potentially broadly neutralizing antibodies [27, 28].

After isolating peripheral blood mononuclear cells (PBMCs), antigen-specific memory B cells were purified using fluorescence-activated cell sorting (FACS) and subjected to single-cell BCR sequencing for paired heavy-light chain mAb sequences. From the PBMCs, we separated $CD19^+$ IgM- $CD27^+$ B cells, which were subsequently stained by HB29-Gn and Gc glycoprotein, and sorted for antigen specificity (Supplementary Fig. 1A). To distinguish between Gn and Gc specificities during sequencing, we labeled each antigen with unique DNA barcodes, which enabled the subsequent retrieval of 1,316 paired heavy-light chain antibody sequences from the stained memory B cells using high-throughput single-cell V(D)J sequencing (scVDJ-seq). Among them, 54 Gn-labeled and 44 Gc-labeled antibody sequences containing immunoglobulin G1 (IgG1) heavy chain constant regions were selected to be expressed *in vitro*. Out of these mAbs tested, 49/54 (90.7%) exhibited binding activity towards the Gn antigen, and 35/44 (79.5%) exhibited binding activity towards the Gc antigen, with varying affinity levels quantified via ELISA (Supplementary Table 2). Then, 49 Gn mAbs and 35 Gc mAbs were further screened for neutralizing activity.

In the neutralization assay, we employed 9 previously established vesicular stomatitis virus (VSV)-based pseudovirus strains, which encompass six major SFTSV genotypes (A-F).[29, 30] These strains include: HB29 (genotype D), HBMC16 (genotype D), WCH (genotype A), HN13 (genotype A), HN20 (genotype F), G/K/2012 (genotype F), SD4 (genotype E), SPL030A (genotype B), and AHL (genotype C). The results show that mAbs against Gn exhibited more potent neutralization

bioRxiv preprint doi: https://doi.org/10.1101/2025.11.26.690690; this version posted November 30, 2025. The copyright holder for this preprint (which was not certified by peer review) is the author/funder, who has granted bioRxiv a license to display the preprint in perpetuity. It is made available under aCC-BY-NC 4.0 International license.

effects against the pseudovirus than those against Gc (Fig. 1C, 1D and Supplementary Table 3), which is consistent with previous reports that neutralizing antibodies against SFTSV primarily target the Gn antigen.[13, 31, 32, 33] The germline information of these mAbs were listed in Supplementary Table 4. Based on these results, mAbs exhibiting broad neutralizing activity were selected for preliminary screening in subsequent authentic virus neutralization assays *in vitro*. From the perspective of the inhibition rate of antibodies against the authentic virus strain HBMC at a concentration of 0.25 μg/ml, 11 mAbs against Gn achieved more than 50% inhibition, and 3 Gn control antibodies (MAb4-5, S2A5, and 40C10) also demonstrated favorable inhibitory effects (Supplementary Fig. 1B). Gc antibodies and SF83 showed almost no inhibition (Supplementary Fig. 1B). We further subjected the 11 Gn antibodies to preliminary screening against other authentic virus strains (SF50, SF53 and WF66), and the results demonstrated that 6 Gn antibodies (BD70-4003, BD70-4008, BD70-4009, BD70-4013, BD70-4017, and BD70-4022) exhibited broadly inhibitory effects (Fig. 1E and Supplementary Table 2). Data basis of heatmap for Fig.1 was listed in Supplementary Table 5, 6, and 7. The majority of these candidates showed high somatic hypermutation (SHM) rates (Supplementary Table 8).

Epitope mapping of mAbs against Gn

Advances in deep antigen mutational screening using a fluorescence-activated cell sorting (FACS)-based yeast display platform have allowed the quick mapping of different antigens with their antibodies, such as SARS-CoV-2[20, 34, 35] and other molecules such as HLA II.[36] For a comprehensive epitope mapping, we build a mutant library of HB29 Gn-head domain. Following a negative selection of the mutant library with each Gn-specific antibody, we performed FACS to isolate yeast cells that failed to bind the respective antibody. These sorted populations were then sequenced to identify critical escape sites for each antibody. Ultimately, antibodies were grouped into the same group if their escape sites were similar or spatially proximate. The Gn mAbs mainly appeared in eight epitope groups (IA-ID, IIA-IIB, IIIA-IIIB), which were determined by unsupervised clustering without dependence on structural studies based on FACS-DMS technology (Fig. 2A and 2B). Detailed information on the amino acid residues for each group can be found in Supplementary Fig. 2. The key amino acid residues on the Gn-head structure for each group and the DMS escape profiles were summarized in Fig. 2B and 2C, respectively. In general, group IA, IC,

bioRxiv preprint doi: https://doi.org/10.1101/2025.11.26.690690; this version posted November 30, 2025. The copyright holder for this preprint (which was not certified by peer review) is the author/funder, who has granted bioRxiv a license to display the preprint in perpetuity. It is made available under aCC-BY-NC 4.0 International license.

and ID mAbs bound to different sites of domain I, while group IIA and IIB mAbs bound to domain II. Another group IB bound to domain I and domain II (Fig. 2B and S2). Group IIIA and IIIB antibodies bound to the domain III of the Gn-head and distributed on amino acids between 260-271 and 271-292, respectively (Fig. 2B and Supplementary Fig. 2). Furthermore, gene analysis of mAbs showed frequent genes involving IGHV5-51/IGHV3-30/IGHV3-15 for the heavy chain and IGKV1-39/IGKV3-15 for the light chain (Fig. 2D).

To elucidate the accuracy of DMS on SFTSV, we compared the DMS results on antibodies that have obtained crystal or cryo-EM structure analysis in previous studies. It has been reported that the interface between the Gn head and MAb4-5 (IIIB) was located on sites 251-256, 275-278, and 284-294 by crystal structure analysis,[12] which was consistent with the key amino acids (287-288, 292) we have screened (Fig. 2B and 2C). For domain I antibodies SF5 (IC) and 40C10 (ID), DMS identified key residues 81-85, 123-126, 171 for SF5, and 64-65, 111-113, 142 for 40C10 (Fig. 2B and 2C). Actually, SF5 (IC) bound to sites 74-90, 121-126, 150-171[37], while 40C10 (ID) bound to sites 62-66, 102, 111-115, 156.[15] Except for site 142, which was close to 65, all sites in this study were consistent with their complex structures. Results of mAbs against domain II were also relatively accurate. According to Ren *et al*'s study,[14] N1D10 (IIA) and B1G11 (IIB) mainly bound to sites 114-121, 218-226, 339-340, and 185-193, 321-323, respectively, which also includes the sites of our DMS results (Fig. 2B and 2C). These data suggest that the SFTSV Gn-head antibody epitope screening system based on yeast mutational library was successful.

To straighten out the relationship between epitopes and function, we conducted a comparative analysis between the DMS epitope grouping and neutralization activities. The results revealed that groups with stronger neutralizing effects were primarily concentrated in IIIA and IA, followed by IIIB. The remaining groups exhibited poor or negligible neutralization activity (Fig. 2E and 2F). Our findings demonstrate a clear direct association between the SFTSV Gn-head domain and mAbs. This approach enables rapid mapping of corresponding epitopes for antibodies of interest.

Protective effect of Gn mAbs *in vitro* and *in vivo*

We employed surface plasmon resonance (SPR) to characterize the binding kinetics of 6 mAbs against HB29-Gn, which demonstrated outstanding performance in preliminary screening (Fig. 1E). Significant variations in the binding affinity between Gn and the mAbs were observed. Among them,

bioRxiv preprint doi: https://doi.org/10.1101/2025.11.26.690690; this version posted November 30, 2025. The copyright holder for this preprint (which was not certified by peer review) is the author/funder, who has granted bioRxiv a license to display the preprint in perpetuity. It is made available under aCC-BY-NC 4.0 International license.

BD70-4008 exhibited the highest binding affinity with an equilibrium dissociation constant (K_D) of 4.77 pM, followed by BD70-4003 with a K_D of 6.73 pM (Supplementary Fig. 3). The mAbs BD70-4009, BD70-4013, BD70-4017, and BD70-4022 displayed binding affinities with K_D values ranging from 0.114 to 1.12 nM (Supplementary Fig. 3). Furthermore, we investigated the neutralizing effects of the 6 antibodies against authentic virus. A focus reduction neutralization test (FRNT) was performed using HBMC16 (genotype D), WCH (genotype A), HNXY2017-50 (genotype D) and HNXY2017-66 (genotype F) (Fig. 3A).[17] All 6 Gn mAbs demonstrated potent neutralization *in vitro* with lower values of $FRNT_{50}$ (Fig. 3B).

To evaluate the prophylactic and therapeutic efficacy of the 6 mAb candidates against SFTSV *in vivo*, *IFNAR1*$^{-/-}$ mice were challenged by SFTSV before or after treatment with the mAb. In prophylactic and therapeutic groups, 5 mg/kg antibody was given to the mice via intraperitoneal (i.p.) injection 1 day pre-infection or 1 day post infection (dpi), respectively (Fig. 3C and 3F). A vehicle group of mice that received phosphate-buffered saline (PBS) was also included. Each group consisted of five or six mice. The body weight of each mouse in each group was monitored and recorded daily. Serum samples were collected from all mice on 3 dpi, with an additional collection performed for the therapeutic group on 5 dpi. And the livers, spleens, and lungs were collected for viral load analyses via qRT-PCR.

In the prophylactic treatment group, most mice died between 5-6 dpi without mAbs injection and exhibited significantly higher viral RNA copies in serum samples (Fig. 3D and 3E). BD70-4003 (IA), BD70-4008 (IIIA), and BD70-4017 (IIIA) protected 100% mice from SFTSV infection, while one mouse died on day 7 or day 10 in the groups treated with BD70-4009 (IIIA), BD70-4013 (IA), and BD70-4022 (IIIA) (Fig. 3D). Viral copy numbers in the serum of mice treated with BD70-4003, BD70-4008, or BD70-4017 were below the detection limit, indicating that these three antibodies exhibit superior efficacy in promoting viral clearance (Fig. 3E). In the therapeutic treatment group, BD70-4003 (IA) and BD70-4017 (IIIA) protected 100% mice from SFTSV challenge (Fig. 3F), and extremely low viral copy numbers were detected in the serum samples collected on both 3 or 5 dpi (Fig. 3H and 3I). The remaining four antibodies conferred weaker protective effects, with varying numbers of deaths occurring within their respective treatment groups. We also analyzed tissue samples collected on 5 dpi. Viral copy numbers in spleens, livers, and lungs from the BD70-4003 and BD70-4017 treatment groups were reduced by 3-4 log values compared to the vehicle group

bioRxiv preprint doi: https://doi.org/10.1101/2025.11.26.690690; this version posted November 30, 2025. The copyright holder for this preprint (which was not certified by peer review) is the author/funder, who has granted bioRxiv a license to display the preprint in perpetuity. It is made available under aCC-BY-NC 4.0 International license.

(Fig. 3J, 3K, and 3L). All these results suggested that administration of either BD70-4003 (IA) or BD70-4017 (IIIA) exhibited significant therapeutic effects. The *in vivo* experimental results further validated our preliminary *in vitro* antibody screening strategy, demonstrating that antibodies targeting epitopes IA and IIIA hold the greatest potential for development as therapeutic antibodies.

Structural analyses of Gn-Ab complexes

To gain deeper insights into the molecular mechanisms underlying the distinct neutralizing activities of different antibodies, we selected 3 mAbs (BD70-4003, BD70-4008, and BD70-4017) for structural analysis. Among them, BD70-4003 and BD70-4008 exhibited competitive binding to Gn protein. Consequently, except Gn head/BD70-4003 Fab and Gn head/BD70-4008 Fab, we also designed 2 combinations of antibodies to form complexes with the Gn-head for structural analysis, to prevent the complex consisting of one Fab and antigen from being too small for structural determination. The Gn head/BD70-4003 Fab and Gn head/BD70-4008 Fab were detected by cryo-EM (Supplementary Table 9), with their structure ultimately resolved at reported global resolution with 2.85 and 2.97 Å, respectively (Supplementary Fig. 4A and 4B). Two complexes, Gn head/BD70-4003 Fab/BD70-4017 Fab and Gn head/BD70-4008 Fab/BD70-4017 Fab, were also resolved with both 2.69 Å resolution (Supplementary Fig. 4C and 4D). Structural analysis showed that BD70-4003 and BD70-4008 mainly bind to the domain I of Gn-head, while BD70-4017 mainly binds to domain III (Fig. 4). In addition, a small part of the interacting interface of BD70-4008 is also distributed on domain III, while a small part of BD70-4017 is distributed on domain I.

Subsequently, we conducted a detailed analysis of residues at the interacting interface between these Fabs and Gn-head. The residues on the interacting interface of antibody BD70-4003 including S32, K34, Q68, Q73-R74, S145-K147, S158-G161, S163-S164 and L166-S169 (Fig. 4A and 4B). Tight binding is facilitated by 11 hydrogen bonds, of which heavy chains (D55, E100, D101, D104, and Y105) contribute all hydrogen bonds with residues S32, K34, Q73-R74, S160, S163-S164, and L166 from Gn (Fig. 4C). BD70-4008 contacts domain I and domain III regions constituted by 24 residues: I25-S35, C49, R53, Q73-R74, G161, S163-S164, L165 and K260-G264 (Fig. 4D and 4E). For BD70-4008, 6 residues (S54, M103, L104, D106, I107, and E109) from the heavy chain and 6 residues (G28, S29, A31, D49, D50, and T92) from the light chain contribute to the tight binding with residues S32, N33, K34, R53, and Q73-R74 from Gn (Fig. 4F).

bioRxiv preprint doi: https://doi.org/10.1101/2025.11.26.690690; this version posted November 30, 2025. The copyright holder for this preprint (which was not certified by peer review) is the author/funder, who has granted bioRxiv a license to display the preprint in perpetuity. It is made available under aCC-BY-NC 4.0 International license.

The two complex structures, Gn head/BD70-4003 Fab/BD70-4017 Fab and Gn head/BD70-4008 Fab/BD70-4017 Fab, collectively define the epitope of the BD70-4017 antibody (Fig. 4G and 4J). BD70-4017 engages 5 residues (P39-L42 and E46) on domain I and 17 residues (K260-T263, P265, S267-E270, A273-C274, T276-S277, S279-C280 and A301-K302) on domain III of Gn (Fig. 4H). Three residues of BD70-4017 light chain (V31, Y33 and D51) form 4 hydrogen bonds with Gn residues (T263, S267 and S269-E270). Specifically, the other hydrogen bond is formed between T70 of BD70-4017 and the mannose on N63 of Gn (Fig. 4I). Although the amino acid residues on the interacting interface of BD70-4008 and BD70-4017 have a slight overlap, involving 3 residues (G262, T263 and P265), the combination of the two antibodies has little effect on the formation of the Gn head/BD70-4003/BD70-4017 complex (Fig. 4K).

We mapped the epitopes of the three antibodies onto the multiple sequence alignment (MSA) plot and annotated them using distinct fill colors: blue for BD70-4003, orange for BD70-4008, and green for BD70-4017 (Supplementary Fig. 5). Residues involved in interactions with the corresponding antibodies were highlighted with deeper shades of the same color scheme. Circular dots in matching color shades represent the important residues identified by DMS. These results clearly demonstrate that the epitopes targeted by the three antibodies are highly conserved, particularly the residues involved in antibody binding. Importantly, the key epitopes identified by yeast DMS fall within the regions resolved by cryo-EM and are predominantly located near interaction residues, further validating the accuracy of our earlier DMS data. This approach shows great potential for application to other bunyaviruses, paving the way for high-throughput and rapid discovery of novel antibody epitopes and for elucidating their functional characteristics.

To investigate the neutralization mechanisms of BD70-4003, BD70-4008, and BD70-4017, we superimposed the structures of the BD70-4003/BD70-4017-Gn and BD70-4008/BD70-4017-Gn complexes onto the native SFTSV virion structure. Previous studies have shown that Gn-Gc heterodimers form hexon and penton on the surface of SFTSV virions.[11, 38] Our results showed that BD70-4003/BD70-4017 and BD70-4008/BD70-4017 binding sites were located on the surfaces of the hexons or pentons (Fig. 5A and 5B). BD70-4003 or BD70-4008 binds to the top side of the authentic SFTSV virion with an orientation nearly perpendicular to the viral membrane, which may be the key factor contributing to the superior affinity and neutralization effects. Although BD70-4017 binds to a more lateral position, its binding is less affected and experiences minimal steric

bioRxiv preprint doi: https://doi.org/10.1101/2025.11.26.690690; this version posted November 30, 2025. The copyright holder for this preprint (which was not certified by peer review) is the author/funder, who has granted bioRxiv a license to display the preprint in perpetuity. It is made available under aCC-BY-NC 4.0 International license.

hindrance. These results demonstrate that BD70-4003, BD70-4008, and BD70-4017 are promising candidate therapeutics for the treatment of SFTSV infection with different neutralizing epitopes.

Discussion

Currently, the clinical management of SFTS is centered on comprehensive supportive care, including platelet transfusion, intravenous immunoglobulin, and blood purification.[39, 40, 41] Due to the lack of specific and effective antiviral drugs, severe cases can rapidly progress to multiple organ failure, particularly in older patients, with significantly increased mortality rates.[42] In recent years, neutralizing antibodies have emerged as a promising therapeutic strategy for combating viral infections.

In this study, we initially utilized multiple previously constructed pseudoviruses[43] to screen antibodies from SFTSV-infected convalescents. Compared to authentic viruses, pseudoviruses offer advantages including lower strain restrictions, higher detection throughput, and operational convenience, making them suitable for preliminary efficacy screening. Notably, we observed that antibody BD70-4017, which displayed relatively modest performance in the pseudovirus system, demonstrated significantly enhanced neutralizing activity against the authentic virus (Fig. 1). This finding highlights that the VSV-G-based pseudovirus system cannot completely mimic the surface glycoprotein arrangement of authentic SFTSV. Similar observations have been previously reported in studies on both SFTSV[14] and hantavirus.[44] In previous studies, lentiviral systems have been utilized to generate SFTSV pseudoviruses[45, 46]; however, their ability to fully recapitulate authentic viruses remains questionable. Future research should focus on optimizing existing systems or developing novel platforms that accurately mimic the glycoprotein distribution of the authentic virus, thereby enabling high-throughput antibody testing in conventional laboratory settings.

Epitopes are critical to the efficacy of antigen-induced immune responses. We previously established a high-throughput yeast display-based DMS platform to investigate antigenic epitopes and antibody function.[20] This method enables rapid identification of key epitope residues for specific mAb by constructing comprehensive mutant libraries of the antigen and screening for escape mutations. In the current study, we displayed the Gn-head domain on the yeast surface and generated a yeast mutant library. Following screening of 44 Gn antibodies and 7 control antibodies, we categorized the antigenic surface of Gn-head into 8 distinct epitope groups (Fig. 2 and

bioRxiv preprint doi: https://doi.org/10.1101/2025.11.26.690690; this version posted November 30, 2025. The copyright holder for this preprint (which was not certified by peer review) is the author/funder, who has granted bioRxiv a license to display the preprint in perpetuity. It is made available under aCC-BY-NC 4.0 International license.

Supplementary Fig. 2). All the epitopes of the selected control antibodies screened above are located within the crystal or cryo-EM structures of the corresponding antigen-antibody complexes, demonstrating the versatility of our DMS approach and its potential for future application, which will provide new perspectives for elucidating bunyavirus glycoprotein epitopes and guiding antibody and vaccine development [12, 14, 15, 16, 37].

IFNAR1$^{-/-}$ mice, which serve as a lethal infection model for SFTSV, have been used to evaluate the drug efficacy.[17, 47, 48] In our animal experiments, both BD70-4003 and BD70-4017 maintained complete protection even when treatment was initiated 1 dpi (Fig. 3), which highlights BD70-4003 and BD70-4017 as promising therapeutic candidates. However, the limitation remains to be addressed. The effectiveness of BD70-4003 or BD70-4017 against advanced-stage infections has not been fully established, since patients typically present for treatment multiple days after symptoms emerge. Further research should prioritize refining dosing protocols and assessing long-term clinical safety and efficacy.

Structural analysis of the BD70-4008/BD70-4017/Gn complex supports their potential use, indicating that the two antibodies bind to distinct epitopes (Fig. 4). However, in the yeast DMS system, the two antibodies were grouped together, likely because BD70-4008 has only three escape residues (Q50, R74, T263), making its escape profile computationally similar to that of BD70-4017, which has more extensive escape sites (K260, P265, S267, S269-E271). This suggests that although the yeast DMS platform offers high throughput, operational simplicity, and rapid turnaround, it still has limitations and may produce grouping bias when an antibody has few escape residues. Apart from this, the escape residues identified for both BD70-4003 and BD70-4017 by DMS were consistently located within the epitopes resolved by cryo-EM (Supplementary Fig. 5). Furthermore, structural analysis confirmed that both BD70-4003 and BD70-4008 can be combined with BD70-4017. Although a partial overlap was observed between the binding interfaces of BD70-4008 and BD70-4017 (Fig. 4K), this does not impede their simultaneous binding. Simulations using authentic virus particles further support this observation (Fig. 5), demonstrating the therapeutic potential of these two antibodies for treating SFTSV infection through different neutralizing epitopes.

Methods

Plasma donors

bioRxiv preprint doi: https://doi.org/10.1101/2025.11.26.690690; this version posted November 30, 2025. The copyright holder for this preprint (which was not certified by peer review) is the author/funder, who has granted bioRxiv a license to display the preprint in perpetuity. It is made available under aCC-BY-NC 4.0 International license.

Blood samples were collected from 12 convalescent individuals previously infected with SFTSV. All plasma-related experiments were approved by the Ethics Committee of Beijing Ditan Hospital, Capital Medical University (approval no. DTEC-KY2022-022-01). Written informed consent was obtained from all participants in accordance with the Declaration of Helsinki, permitting the collection, storage, and research use of clinical samples, as well as publication of resulting data.

Whole blood samples were diluted 1:1 with PBS containing 2% FBS and subjected to Ficoll (Cytiva, 17-1440-03) density gradient centrifugation to separate plasma and PBMCs. Plasma was collected from the upper layer, while cells at the interface were harvested for PBMC isolation. PBMCs were further processed by centrifugation, red blood cell lysis (Invitrogen eBioscience 1× RBC Lysis Buffer, 00-4333-57), and washing steps. Samples not used immediately were were stored in FBS (Gibco) containing 10% DMSO (Sigma) in liquid nitrogen. Cryopreserved PBMCs were thawed in DPBS containing 2% FBS (Stemcell, 07905) prior to use.

Antigen-specific cell sorting, V(D)J sequencing, and data analysis

PBMCs were processed using the EasySep Human CD19 Positive Selection Kit II (STEMCELL, 17854) to isolate $CD19^+$ B cells. Cells were stained with FITC anti-human CD19 (BioLegend, 302206, clone HIB19), Brilliant Violet 421 anti-human CD27 (BioLegend, 302824, clone O323), and PE/Cyanine7 anti-human IgM (BioLegend, 314532, clone MHM-88). For antigen labeling, biotinylated SFTSV HB29-Gn or HB29-Gc protein was conjugated with PE-streptavidin (BioLegend, 405204) and APC-streptavidin (BioLegend, 405207), respectively. Biotinylated ovalbumin (OVA; Sino Biological) conjugated with streptavidin served as a negative control. Specifically, HB29-Gn and HB29-Gc were labeled with distinct barcodes: Gn was conjugated with TotalSeq™-C0971 and TotalSeq™-C0972 Streptavidin (BioLegend, 405271 and 405273), while Gc was conjugated with TotalSeq™-C0973 and TotalSeq™-C0974 Streptavidin (BioLegend, 405275 and 405277) to enable sequencing-adapted sorting. OVA was labeled with TotalSeq™-C0975 Streptavidin (BioLegend, 405279). Cells were incubated on ice in the dark for 30 minutes and washed twice. Dead cells were excluded by 7-AAD staining (Invitrogen, 00-6993-50). $7\text{-}AAD^-$, $CD19^+$, $CD27^+$, IgM^-, OVA^-, and antigen-positive (Gn^+ or Gc^+) B cells were sorted using a MoFlo Astrios EQ Cell Sorter (Beckman Coulter). FACS data were acquired with Summit 6.0 (Beckman

bioRxiv preprint doi: https://doi.org/10.1101/2025.11.26.690690; this version posted November 30, 2025. The copyright holder for this preprint (which was not certified by peer review) is the author/funder, who has granted bioRxiv a license to display the preprint in perpetuity. It is made available under aCC-BY-NC 4.0 International license.

Coulter) and analyzed using FlowJo v10.8 (BD Biosciences).

Sorted cells were processed using the 10X Genomics Chromium Next GEM Single Cell V(D)J kit (v1.1, CG000208) according to the manufacturer's protocol to generate barcoded libraries via GEM formation, reverse transcription, and cDNA amplification. Libraries were sequenced on an Illumina platform.

BCR contigs were assembled and aligned to the reference using Cell Ranger (v6.1.1). Only productive contigs and B cells with paired heavy and light chains were retained after quality filtering. Germline V(D)J gene annotation was performed with IgBlast (v1.17.1), and somatic hypermutations were analyzed using the Change-O toolkit (v1.2.0).

Monoclonal antibody expression and purification

Human antibody heavy- and light-chain genes were synthesized and cloned into respective pCMV3 vectors (pCMV3-CH, pCMV3-CL, or pCMV3-CK). Following transformation into E. coli DH5α (Tsingke, TSC-C01-96) and overnight incubation at 37°C, positive clones were identified by colony PCR and Sanger sequencing, followed by plasmid preparation (CWBIO, CW2105). For protein expression, Expi293F cells were co-transfected with paired plasmids using PEI (Yeasen, 40816ES03) in 0.9% NaCl. Transfected cultures were maintained under standard growth conditions, with nutrient supplement (OPM Biosciences, F081918-001) added 24 h post-transfection and replenished every 48 h. Supernatants were harvested after 8 days of culture for antibody purification.

Antibodies were purified from clarified supernatant (3,000 × g, 10 min) using Protein A magnetic beads (GenScript, L00695) and a KingFisher system (Thermo Fisher). Final samples were quantified by NanoDrop (Thermo Fisher, 840-317400) and analyzed for purity by SDS-PAGE (LabLead, P42015).

ELISA

Purified SFTSV Gn or Gc proteins (1 μg/mL in Solarbio C1055 buffer) were used to coat ELISA plates overnight at 4°C. After washing and blocking, serially diluted antibodies were added and incubated for 30 minutes at room temperature. The plates were then incubated with an HRP-conjugated goat anti-human IgG (Jackson ImmunoResearch, 109-035-003; 0.25 μg/mL) for 30 minutes, followed by tetramethylbenzidine (TMB) substrate (Solarbio, PR1200) for signal

bioRxiv preprint doi: https://doi.org/10.1101/2025.11.26.690690; this version posted November 30, 2025. The copyright holder for this preprint (which was not certified by peer review) is the author/funder, who has granted bioRxiv a license to display the preprint in perpetuity. It is made available under aCC-BY-NC 4.0 International license.

development. The reaction was terminated with H_2SO_4, and absorbance at 450 nm was read on a microplate reader (Multiskan Fc, Thermo Scientific).

Surface Plasmon Resonance

SPR experiments were performed on a Biacore 8K (Cytiva). SFTSV mAbs (human IgG1) were captured by a Sensor Chip Protein A (Cytiva). Various concentrations of SFTSV Gn (His-tag; 1.5625, 3.125, 6.25, 12.5, 25, and 50 nM) were injected. The response was recorded at room temperature, and the raw data curves were fitted to a 1:1 binding model using Biacore Insight Evaluation Software (Cytiva, v4.0.8).

Pseudovirus neutralisation assay

SFTSV Gn/Gc pseudoviruses were produced using a VSV-based system. Briefly, 293T cells were infected with G*ΔG-VSV (Kerafast) and transfected with a plasmid encoding the SFTSV glycoproteins. The culture supernatant containing the pseudoviruses was collected, clarified by filtration, aliquoted, and stored at -80°C. For the neutralization assay, serially diluted monoclonal antibodies were mixed with pseudoviruses and incubated for 1 hour at 37°C with 5% CO_2. Huh-7 cells were then added to the mixture. After 48 hours, the supernatant was removed, and luminescence was measured following the addition of D-luciferin substrate (PerkinElmer, 6066769) using a microplate reader (PerkinElmer, HH3400). The half-maximal inhibitory concentration (IC_{50}) was determined by fitting the data to a four-parameter logistic model in GraphPad Prism (v9.0.1).

DMS library construction

DMS libraries were constructed as previously described, with modifications for the SFTSV Gn-head domain (residues 20-340). Using the HB29 Gn-head coding sequence as a template, two independent mutant libraries were generated via three rounds of mutagenesis PCR with synthesized primer pools. Each Gn-head variant was constructed with an N-terminal HA tag and a C-terminal MYC tag, linked to a unique 26-nucleotide barcode. Barcode-variant mapping was performed by PacBio sequencing. The mutant libraries were cloned into the pETcon vector and electroporated into DH10B cells for plasmid amplification. Plasmids were then transformed into the EBY100 strain of Saccharomyces cerevisiae as previously reported.[49] Transformed yeast were selected on SD-CAA

bioRxiv preprint doi: https://doi.org/10.1101/2025.11.26.690690; this version posted November 30, 2025. The copyright holder for this preprint (which was not certified by peer review) is the author/funder, who has granted bioRxiv a license to display the preprint in perpetuity. It is made available under aCC-BY-NC 4.0 International license.

plates and expanded in SD-CAA liquid medium. Yeast libraries were flash-frozen in liquid nitrogen and stored at -80°C.

High-throughput antibody-escape profiling

Antibody escape mutations were assessed using a FACS-based workflow. Yeast-expressing Gn-head mutants were induced overnight and stained. After incubation with primary Gn mAbs for 30 minutes at 4°C, cells were stained with secondary antibodies: APC anti-HA.11 (BioLegend, 901524), FITC-conjugated chicken anti-c-Myc (icllab, CMYC-45F), and PE-conjugated goat anti-human IgG (Jackson, 109-115-098) for 30 minutes at 4°C. Double-positive (MYC^+ HA^+) yeast displaying bound mAbs were gated, and mAb-unbound populations adjacent to the main population were sorted and collected. Plasmid DNA was extracted after 40 hours of culture, barcodes were PCR-amplified, purified with AMPure XP beads (Beckman Coulter, A63882), and subjected to high-throughput sequencing on an Illumina NovaSeq X Plus platform.

Processing of DMS data

Illumina single-end sequencing reads from Gn-head DMS libraries were processed as described with minor modifications. Raw reads were trimmed to 26 bp and mapped to a barcode-variant dictionary using the dms_variants package (v0.8.9). Variant escape scores were calculated as $F \times (n_{X,ab}/N_{ab})/(n_{X,ref}/N_{ref})$, where $n_{X,ab}$ and $n_{X,ref}$ is the number of reads representing variant X, and N_{ab} and N_{ref} are the total number of valid reads in antibody-selected (ab) and reference (ref) library, respectively. F is a normalization factor defined as the 99th percentile of escape fraction ratios. Variants with fewer than six reads in the reference library or those associated with severely impaired Gn-head expression were excluded. Global epistasis models were fitted using dms_variants to infer per-mutation escape scores. Escape scores were averaged across replicates that passed quality control.

Site-level escape scores were computed as the sum of mutation escape scores per Gn-head residue. These scores were used as antibody-specific features to generate a matrix $A_{N\times M}$, where N is the number of antibodies and M is the number of valid positions. Non-surface residues on Gn-head were removed from the analysis. We calculated the pairwise similarities, defined as the square root of the Jensen-Shannon divergence (scipy, v1.11.2) between the feature vectors of two antibodies.

bioRxiv preprint doi: https://doi.org/10.1101/2025.11.26.690690; this version posted November 30, 2025. The copyright holder for this preprint (which was not certified by peer review) is the author/funder, who has granted bioRxiv a license to display the preprint in perpetuity. It is made available under aCC-BY-NC 4.0 International license.

The dissimilarity (1.0 - similarity) matrix were used to build a k-nearest neighbor graph (k = 6) and clustered into epitope groups using Leiden algorithm (leidenalg, v0.10.2).

Authentic virus neutralization assay

Neutralizing activity of mAbs against authentic SFTSV was measured using a FRNT. The four representative SFTSV strains used for testing include HBMC16, WCH, HNXY2017-50, and HNXY2017-66.[17] Briefly, serially diluted mAbs were incubated with SFTSV virions for 1 hour at 37°C. The mixture was added to Vero cells and incubated for 1.5 hours at 37°C. Cells were then cultured for 3.5 days in DMEM containing 1.25% methylcellulose. After fixation with 3.7% paraformaldehyde for 30 minutes, cells were stained with an anti-SFTSV NP primary antibody, followed by an HRP-conjugated anti-mouse secondary antibody (Applygen, C1308). Staining was developed using a DAB substrate (TIANGEN, PA110). Plaque numbers were recorded, and $FRNT_{50}$ values were calculated.

***In vivo* SFTSV Challenge Experiment**

Mouse studies were conducted as previously described.[17] To assess the prophylactic efficacy, *IFNAR1*$^{-/-}$ mice received a single intraperitoneal (IP) injection of 5 mg/kg of each mAb or a human IgG1 isotype control antibody one day before IP inoculation with 20 FFUs of SFTSV HBMC16. Mice were monitored daily for clinical signs, body weight, and mortality for over 12 days. Weight data are expressed as percentages of initial weight. Serum samples were collected at 3 days post-infection (dpi) for viral load analysis. The therapeutic assessment was largely identical to the prophylactic experiment described above, except that administration occurred one day post-infection. Serum was collected at 3 and 5 dpi for viral load quantification. At 5 dpi, four mice per group were euthanized, and spleen, lung, and liver samples were harvested for viral load determination.

RT-qPCR assay

Total RNA from tissues was extracted using the RNAprep Pure Cell Kit (TIANGEN, DP430). Intracellular viral RNA was quantified by RT-qPCR targeting the SFTSV L segment with primes: SFTSV-L-F: 5′-CTCACTCATGCCCTCAACGA-3′ and SFTSV-L-R: 5′-

bioRxiv preprint doi: https://doi.org/10.1101/2025.11.26.690690; this version posted November 30, 2025. The copyright holder for this preprint (which was not certified by peer review) is the author/funder, who has granted bioRxiv a license to display the preprint in perpetuity. It is made available under aCC-BY-NC 4.0 International license.

GATGAACTCACCAGCCCTGC-3′. For serum samples, RNA was extracted with the TIANamp Virus RNA Kit (TIANGEN, DP315-R), and viral load was quantified using primers targeting the SFTSV S segment: SFTSV-S-F: 5′-AGCCTAATTGGATATGTCAAATTGC-3′ and SFTSV-S-R: 5′-CGGGTGAAGTGGCTGAAGG-3′.

Protein expression and purification for structural analysis

Expression constructs encoding the ectodomains of SFTSV Gn or Gc were transiently transfected into HEK293F cells using polyethylenimine (Polysciences). Culture supernatants were harvested 7 days post-transfection, concentrated, and exchanged into binding buffer (25 mM Tris-HCl, pH 8.0, 200 mM NaCl). Proteins were first purified by Ni-NTA affinity chromatography, followed by size-exclusion chromatography on a Superose 6 Increase column in final buffer (20 mM HEPES, pH 7.2, 150 mM NaCl). The Gn-head domain was expressed and purified similarly. Antibody Fabs were expressed and purified as previously described.[50]

Cryo-EM sample preparation, data collection and model building

For the preparation of the complexes, the purified HB29-Gn-head was mixed with a 1.5-fold molar excess of fab BD70-4003 and BD70-4017, BD70-4008-fab and BD70-4017, BD70-4003, BD70-4008-fab separately, incubated on ice for 40 min and injected onto a Superdex 200 Increase 5/150 column (Cytiva) equilibrated with buffer 1× PBS. SDS-PAGE analysis confirmed the formation of the HB29-Gn-head-3-17, HB29-Gn-head-8-17, HB29-Gn-head-3, HB29-Gn-head-8 complexes in a stoichiometric ratio respectively.

An aliquot of 4 μL protein sample of complex at a protein concentration of 0.5 mg/mL was loaded onto a glow-discharged 300 mesh grid (Quantifoil Au R1.2/1.3). The grids were blotted with a filter paper at 4 ℃ and 100% humidity,[51] and flash-cooled in liquid ethane using a Thermo Fisher Vitrobot Mark IV and screened using a 200 KV Talos Aectica.

Cryo-EM datasets were collected on a 300kV Thermo Fisher Titan Krios G4 electron microscope equipped with a Falcon 4 camera and a selectris X energy filter (GIF: a slit width of 10eV). The micrographs were collected at a calibrated magnification of x130,000 using the EPU software (Thermo Fisher Scientific), yielding a pixel size of 0.95 Å at object scale. Movies were recorded at an accumulated electron dose of 60e^{-}Å^{-2} s^{-1} on each micrograph that was fractionated

bioRxiv preprint doi: https://doi.org/10.1101/2025.11.26.690690; this version posted November 30, 2025. The copyright holder for this preprint (which was not certified by peer review) is the author/funder, who has granted bioRxiv a license to display the preprint in perpetuity. It is made available under aCC-BY-NC 4.0 International license.

into a stack of 40 frames with a defocus range of -1.0 μm to -2.0 μm.

Data processing was performed using cryoSPARC (v4.7.1).[52] The data underwent several steps including Motion Correction, CTF Estimation, Create Templates, Template Picker, Extract from Micrographs, 2D classification, 2D selection for Ab-initio Reconstruction, and subsequent Homogeneous Refinement. To enhance the density around the HB29-Gn-head-Fab region, local refinement was conducted using UCSF ChimeraX (v1.7)[53] and cryoSPARC. Structural modeling and refinement were performed using WinCoot (v0.9.4.1)[54] and Phenix (v1.21.2).[55] Figures were generated using UCSF ChimeraX (v1.7).[56]

References

1. Yu XJ, *et al.* Fever with thrombocytopenia associated with a novel bunyavirus in China. *N Engl J Med* **364**, 1523-1532 (2011).
2. Liu W, *et al.* Case-fatality ratio and effectiveness of ribavirin therapy among hospitalized patients in china who had severe fever with thrombocytopenia syndrome. *Clin Infect Dis* **57**, 1292-1299 (2013).
3. Liu Q, He B, Huang SY, Wei F, Zhu XQ. Severe fever with thrombocytopenia syndrome, an emerging tick-borne zoonosis. *Lancet Infect Dis* **14**, 763-772 (2014).
4. Yang T, Huang H, Jiang L, Li J. Overview of the immunological mechanism underlying severe fever with thrombocytopenia syndrome (Review). *Int J Mol Med* **50**, (2022).
5. Wang Y, *et al.* Clinical laboratory parameters and fatality of Severe fever with thrombocytopenia syndrome patients: A systematic review and meta-analysis. *PLoS Negl Trop Dis* **16**, e0010489 (2022).
6. Egizi A, *et al.* First glimpse into the origin and spread of the Asian longhorned tick, Haemaphysalis longicornis, in the United States. *Zoonoses Public Health* **67**, 637-650 (2020).
7. Miao D, *et al.* Mapping the global potential transmission hotspots for severe fever with thrombocytopenia syndrome by machine learning methods. *Emerg Microbes Infect* **9**, 817-826 (2020).
8. Zhang X, *et al.* Rapid Spread of Severe Fever with Thrombocytopenia Syndrome Virus by Parthenogenetic Asian Longhorned Ticks. *Emerg Infect Dis* **28**, 363-372 (2022).
9. Spiegel M, Plegge T, Pohlmann S. The Role of Phlebovirus Glycoproteins in Viral Entry, Assembly and Release. *Viruses* **8**, (2016).
10. Halldorsson S, *et al.* Structure of a phleboviral envelope glycoprotein reveals a consolidated model of membrane fusion. *Proc Natl Acad Sci U S A* **113**, 7154-7159 (2016).
11. Du S, *et al.* Cryo-EM structure of severe fever with thrombocytopenia syndrome virus. *Nat Commun* **14**, 6333 (2023).
12. Wu Y, *et al.* Structures of phlebovirus glycoprotein Gn and identification of a neutralizing antibody epitope. *Proc Natl Acad Sci U S A* **114**, E7564-E7573 (2017).
13. Kim KH, *et al.* An anti-Gn glycoprotein antibody from a convalescent patient potently inhibits the infection of severe fever with thrombocytopenia syndrome virus. *PLoS Pathog* **15**, e1007375 (2019).

bioRxiv preprint doi: https://doi.org/10.1101/2025.11.26.690690; this version posted November 30, 2025. The copyright holder for this preprint (which was not certified by peer review) is the author/funder, who has granted bioRxiv a license to display the preprint in perpetuity. It is made available under aCC-BY-NC 4.0 International license.

14. Ren X, *et al.* A broadly protective antibody targeting glycoprotein Gn inhibits severe fever with thrombocytopenia syndrome virus infection. *Nat Commun* **15**, 7009 (2024).
15. Yang P, *et al.* Molecular mechanism and structure-guided humanization of a broadly neutralizing antibody against SFTSV. *PLoS Pathog* **20**, e1012550 (2024).
16. Wu X, *et al.* Identification and characterization of three monoclonal antibodies targeting the SFTSV glycoprotein and displaying a broad spectrum recognition of SFTSV-related viruses. *PLoS Negl Trop Dis* **18**, e0012216 (2024).
17. Zhang S, *et al.* Discovery and characterization of potent broadly neutralizing antibodies from human survivors of severe fever with thrombocytopenia syndrome. *EBioMedicine* **111**, 105481 (2025).
18. Quan C, *et al.* Molecular mechanism of potently neutralizing human monoclonal antibodies against severe fever with thrombocytopenia virus infection. *J Virol* **99**, e0053325 (2025).
19. Greaney AJ, *et al.* Complete Mapping of Mutations to the SARS-CoV-2 Spike Receptor-Binding Domain that Escape Antibody Recognition. *Cell Host Microbe* **29**, 44-57 e49 (2021).
20. Cao Y, *et al.* Omicron escapes the majority of existing SARS-CoV-2 neutralizing antibodies. *Nature* **602**, 657-663 (2022).
21. Jian F, *et al.* Evolving antibody response to SARS-CoV-2 antigenic shift from XBB to JN.1. *Nature* **637**, 921-929 (2025).
22. Yisimayi A, *et al.* Repeated Omicron exposures override ancestral SARS-CoV-2 immune imprinting. *Nature* **625**, 148-156 (2024).
23. Cao Y, *et al.* Imprinted SARS-CoV-2 humoral immunity induces convergent Omicron RBD evolution. *Nature* **614**, 521-529 (2023).
24. Cao Y, *et al.* BA.2.12.1, BA.4 and BA.5 escape antibodies elicited by Omicron infection. *Nature* **608**, 593-602 (2022).
25. Cao Y, *et al.* Rational identification of potent and broad sarbecovirus-neutralizing antibody cocktails from SARS convalescents. *Cell Rep* **41**, 111845 (2022).
26. Jian F, *et al.* Viral evolution prediction identifies broadly neutralizing antibodies to existing and prospective SARS-CoV-2 variants. *Nat Microbiol* **10**, 2003-2017 (2025).
27. Chung H, *et al.* Kinetics of Glycoprotein-Specific Antibody Response in Patients with Severe Fever with Thrombocytopenia Syndrome. *Viruses* **14**, (2022).
28. Li JC, *et al.* Dynamics of neutralizing antibodies against severe fever with thrombocytopenia syndrome virus. *Int J Infect Dis* **134**, 95-98 (2023).
29. Fu Y, *et al.* Phylogeographic analysis of severe fever with thrombocytopenia syndrome virus from Zhoushan Islands, China: implication for transmission across the ocean. *Sci Rep* **6**, 19563 (2016).
30. Yun SM, *et al.* Molecular genomic characterization of tick- and human-derived severe fever with thrombocytopenia syndrome virus isolates from South Korea. *PLoS Negl Trop Dis* **11**, e0005893 (2017).
31. Guo X, *et al.* Human antibody neutralizes severe Fever with thrombocytopenia syndrome virus, an emerging hemorrhagic Fever virus. *Clin Vaccine Immunol* **20**, 1426-1432 (2013).
32. Park SY, *et al.* Use of Plasma Therapy for Severe Fever with Thrombocytopenia Syndrome Encephalopathy. *Emerg Infect Dis* **22**, 1306-1308 (2016).
33. Choi S, Kim MC, Kwon JS, Kim JY, Lee KH, Kim SH. Case Report: Use of Plasma Exchange Followed by Convalescent Plasma Therapy in a Critically Ill Patient with Severe Fever and

bioRxiv preprint doi: https://doi.org/10.1101/2025.11.26.690690; this version posted November 30, 2025. The copyright holder for this preprint (which was not certified by peer review) is the author/funder, who has granted bioRxiv a license to display the preprint in perpetuity. It is made available under aCC-BY-NC 4.0 International license.

Thrombocytopenia Syndrome-Associated Encephalopathy: Cytokine/Chemokine Concentrations, Viral Loads, and Antibody Responses. *Am J Trop Med Hyg* **99**, 1466-1468 (2018).

34. Starr TN, *et al.* Prospective mapping of viral mutations that escape antibodies used to treat COVID-19. *Science* **371**, 850-854 (2021).
35. Starr TN, Greaney AJ, Dingens AS, Bloom JD. Complete map of SARS-CoV-2 RBD mutations that escape the monoclonal antibody LY-CoV555 and its cocktail with LY-CoV016. *Cell Rep Med* **2**, 100255 (2021).
36. Sivelle C, *et al.* Combining deep mutational scanning to heatmap of HLA class II binding of immunogenic sequences to preserve functionality and mitigate predicted immunogenicity. *Front Immunol* **14**, 1197919 (2023).
37. Chang Z, *et al.* Bispecific antibodies targeting two glycoproteins on SFTSV exhibit synergistic neutralization and protection in a mouse model. *Proc Natl Acad Sci U S A* **121**, e2400163121 (2024).
38. Sun Z, *et al.* Architecture of severe fever with thrombocytopenia syndrome virus. *Protein Cell* **14**, 914-918 (2023).
39. Zhai Y, *et al.* Intravenous immunoglobulin-based adjuvant therapy for severe fever with thrombocytopenia syndrome: A single-center retrospective cohort study. *J Med Virol* **96**, e70017 (2024).
40. Song X, Xu X, Ren X, Ruan X, Bo J. Therapeutic plasma exchange combined with ribavirin to rescue critical SFTS patients. *J Clin Apher* **39**, e22131 (2024).
41. Wang W, Zhang A, Wu Q, Zhu L, Yang J. Epidemiological and Clinical Characteristics of Severe Fever with Thrombocytopenia Syndrome in Southern Anhui Province, China, 2011-2020. *Jpn J Infect Dis* **75**, 133-139 (2022).
42. Zu Z, *et al.* A ten-year assessment of the epidemiological features and fatal risk factors of hospitalised severe fever with thrombocytopenia syndrome in Eastern China. *Epidemiol Infect* **150**, e131 (2022).
43. Xu J, *et al.* Analysis of cross neutralizing activity of antibodies from sera of severe fever with thrombocytopenia syndrome patients to deal with different genotype strains. *Front Microbiol* **13**, 1020545 (2022).
44. Engdahl TB, *et al.* Antigenic mapping and functional characterization of human New World hantavirus neutralizing antibodies. *Elife* **12**, (2023).
45. Hofmann H, *et al.* Severe fever with thrombocytopenia virus glycoproteins are targeted by neutralizing antibodies and can use DC-SIGN as a receptor for pH-dependent entry into human and animal cell lines. *J Virol* **87**, 4384-4394 (2013).
46. Chen R, Huang W, Wang Y. Pseudotyped Virus for Bandavirus. *Adv Exp Med Biol* **1407**, 265-277 (2023).
47. Matsuno K, *et al.* Animal Models of Emerging Tick-Borne Phleboviruses: Determining Target Cells in a Lethal Model of SFTSV Infection. *Front Microbiol* **8**, 104 (2017).
48. Tani H, *et al.* Efficacy of T-705 (Favipiravir) in the Treatment of Infections with Lethal Severe Fever with Thrombocytopenia Syndrome Virus. *mSphere* **1**, (2016).
49. Gietz RD, Schiestl RH. High-efficiency yeast transformation using the LiAc/SS carrier DNA/PEG method. *Nat Protoc* **2**, 31-34 (2007).
50. Du S, *et al.* Structurally Resolved SARS-CoV-2 Antibody Shows High Efficacy in Severely

bioRxiv preprint doi: https://doi.org/10.1101/2025.11.26.690690; this version posted November 30, 2025. The copyright holder for this preprint (which was not certified by peer review) is the author/funder, who has granted bioRxiv a license to display the preprint in perpetuity. It is made available under aCC-BY-NC 4.0 International license.

Infected Hamsters and Provides a Potent Cocktail Pairing Strategy. *Cell* **183**, 1013-1023 e1013 (2020).

51. Du S, *et al.* Structures of SARS-CoV-2 B.1.351 neutralizing antibodies provide insights into cocktail design against concerning variants. *Cell Res* **31**, 1130-1133 (2021).
52. Punjani A, Rubinstein JL, Fleet DJ, Brubaker MA. cryoSPARC: algorithms for rapid unsupervised cryo-EM structure determination. *Nat Methods* **14**, 290-296 (2017).
53. Pettersen EF, *et al.* UCSF Chimera--a visualization system for exploratory research and analysis. *J Comput Chem* **25**, 1605-1612 (2004).
54. Emsley P, Lohkamp B, Scott WG, Cowtan K. Features and development of Coot. *Acta Crystallogr D Biol Crystallogr* **66**, 486-501 (2010).
55. Liebschner D, *et al.* Macromolecular structure determination using X-rays, neutrons and electrons: recent developments in Phenix. *Acta Crystallogr D Struct Biol* **75**, 861-877 (2019).
56. Pettersen EF, *et al.* UCSF ChimeraX: Structure visualization for researchers, educators, and developers. *Protein Sci* **30**, 70-82 (2021).

Acknowledgments

We thank Yantai Qishan Hospital for the assistance in recruiting SFTSV-infected convalescents and collecting samples. We thank Yuhang Wang from Changping Laboratory for the support of structure analysis. We thank Nanjing GenScript Biotechnology for the technical assistance on the purification of mAbs. This project is financially supported by Changping Laboratory (2025D-04-01).

Author contributions

Y.C. designed the study. Y.C., Q.W., and J.L. wrote the manuscript with input from all authors. Y.C. and F.S. coordinated the expression and characterization of the neutralizing antibodies. F.J., Q.W., and H.S. performed and analyzed the yeast display screening experiments. Q.W., Y.Y., J.W., L.Y., and Y.W. performed the neutralizing antibody expression and characterization, including pseudovirus neutralization assays and ELISA. Q.W., M.M, and F.J. performed and analyzed the antigen-specific single B cell VDJ sequencing. Y.W. and Q.W. performed the structural analyses. W.L., H.L. and A.H. performed and coordinated the authentic virus neutralization and animal experiments. Y.L. and L.Z. recruited the SFTSV convalescents.

Declaration of interests

Provisional patents related to the antibodies identified in this paper have been filed. Y.C. is the co-founder of Singlomics Biopharmaceuticals.

bioRxiv preprint doi: https://doi.org/10.1101/2025.11.26.690690; this version posted November 30, 2025. The copyright holder for this preprint (which was not certified by peer review) is the author/funder, who has granted bioRxiv a license to display the preprint in perpetuity. It is made available under aCC-BY-NC 4.0 International license.

Materials & Correspondence

All data and materials presented in this manuscript are available from the lead contact upon a reasonable request under a completed Material Transfer Agreement. Further information and requests for resources and reagents should be directed to and will be fulfilled by the lead contact, yunlongcao@pku.edu.cn (Y.C.).

Supplementary Information

Supplementary Fig. 1. Isolate memory B cells from SFTSV infected convalescent plasma and screening of mAbs
Related to Fig. 1.

Supplementary Fig. 2. Average escape scores of antibodies in eight groups
Related to Fig. 2.

Supplementary Fig. 3. Antigen affinity of Gn-reactive mAbs
Related to Fig. 3.

Supplementary Fig. 4. Workflow for the cryo-EM 3D reconstruction
Related to Fig. 4.

Supplementary Fig. 5. Sequence alignment of BD70-4003, BD70-4008, and BD70-4017 epitopes
Related to Fig. 4.

Supplementary Table 1. Summarized information of SFTSV-infected convalescents

Supplementary Table 2. Binding capabilities of SFTSV-Gn or Gc antibodies

Supplementary Table 3. Neutralizing activities of SFTSV-Gn or Gc antibodies

Supplementary Table 4. Germline and CDR3 sequences of SFTSV-Gn or Gc antibodies

Supplementary Table 5. Source data of the heatmap in Fig. 1C

Supplementary Table 6. Source data of the heatmap in Fig. 1D

Supplementary Table 7. Source data of the heatmap in Fig. 1E

Supplementary Table 8. SHM counts and rates in nucleotides in addition to the germline V-J gene combinition of the 6 antibodies

Supplementary Table 9. Cryo-EM data collection, refinement and validation statistics

bioRxiv preprint doi: https://doi.org/10.1101/2025.11.26.690690; this version posted November 30, 2025. The copyright holder for this preprint (which was not certified by peer review) is the author/funder, who has granted bioRxiv a license to display the preprint in perpetuity. It is made available under aCC-BY-NC 4.0 International license.

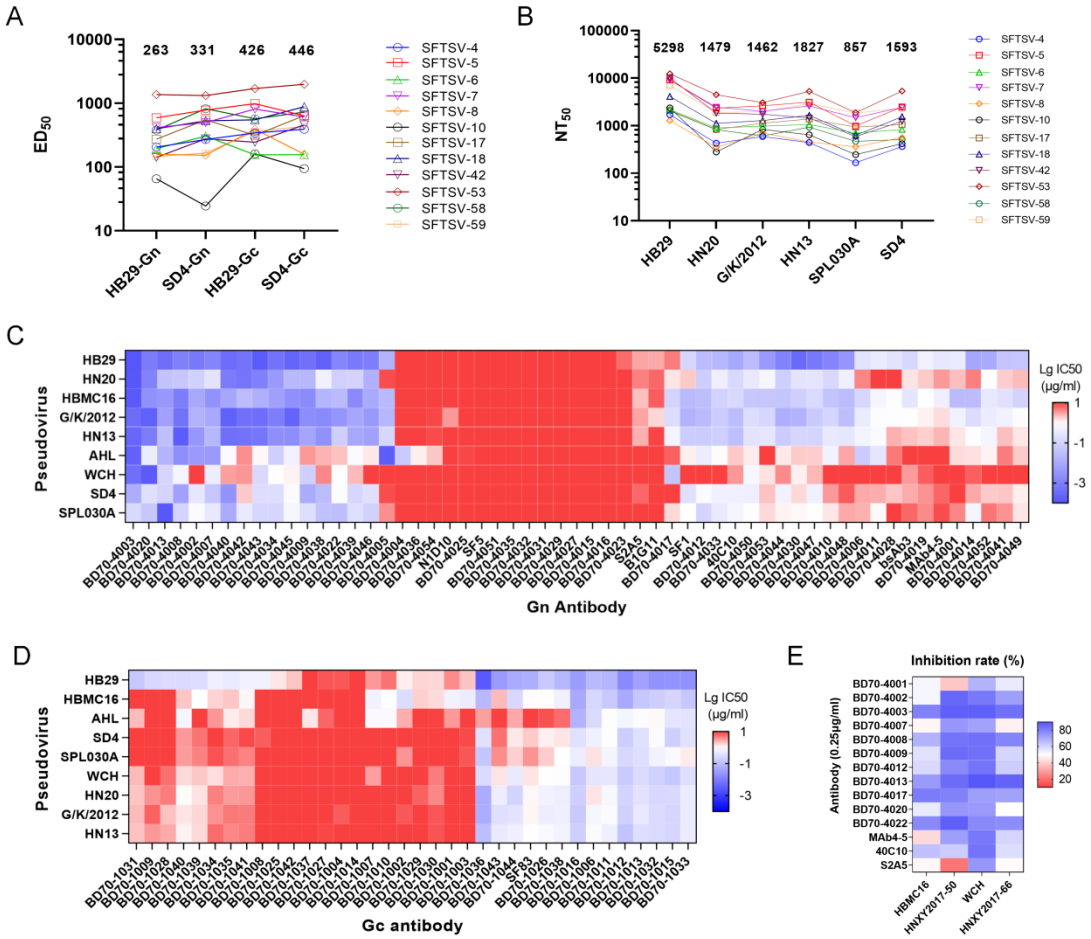

Fig. 1. Identification of broad neutralizing antibodies from SFTSV-infected convalescents

(A) The median effective dose (ED_{50}) of plasma from SFTSV-infected convalescents was determined by ELISA. The average value of each group was marked.

(B) The half maximal neutralization titre (NT_{50}) of plasma against VSV-based SFTSV pseudoviruses.

(C-D) Neutralizing median inhibition concentration (IC_{50}, μg/ml) of SFTSV Gn (C) or Gc (D) antibodies using VSV-based pseudoviruses. Neutralization assays were conducted in at least two biological replicates.

(E) The inhibition rate of 14 selected mAbs against four SFTSV authentic viruses at a dose of 0.25μg/ml.

bioRxiv preprint doi: https://doi.org/10.1101/2025.11.26.690690; this version posted November 30, 2025. The copyright holder for this preprint (which was not certified by peer review) is the author/funder, who has granted bioRxiv a license to display the preprint in perpetuity. It is made available under aCC-BY-NC 4.0 International license.

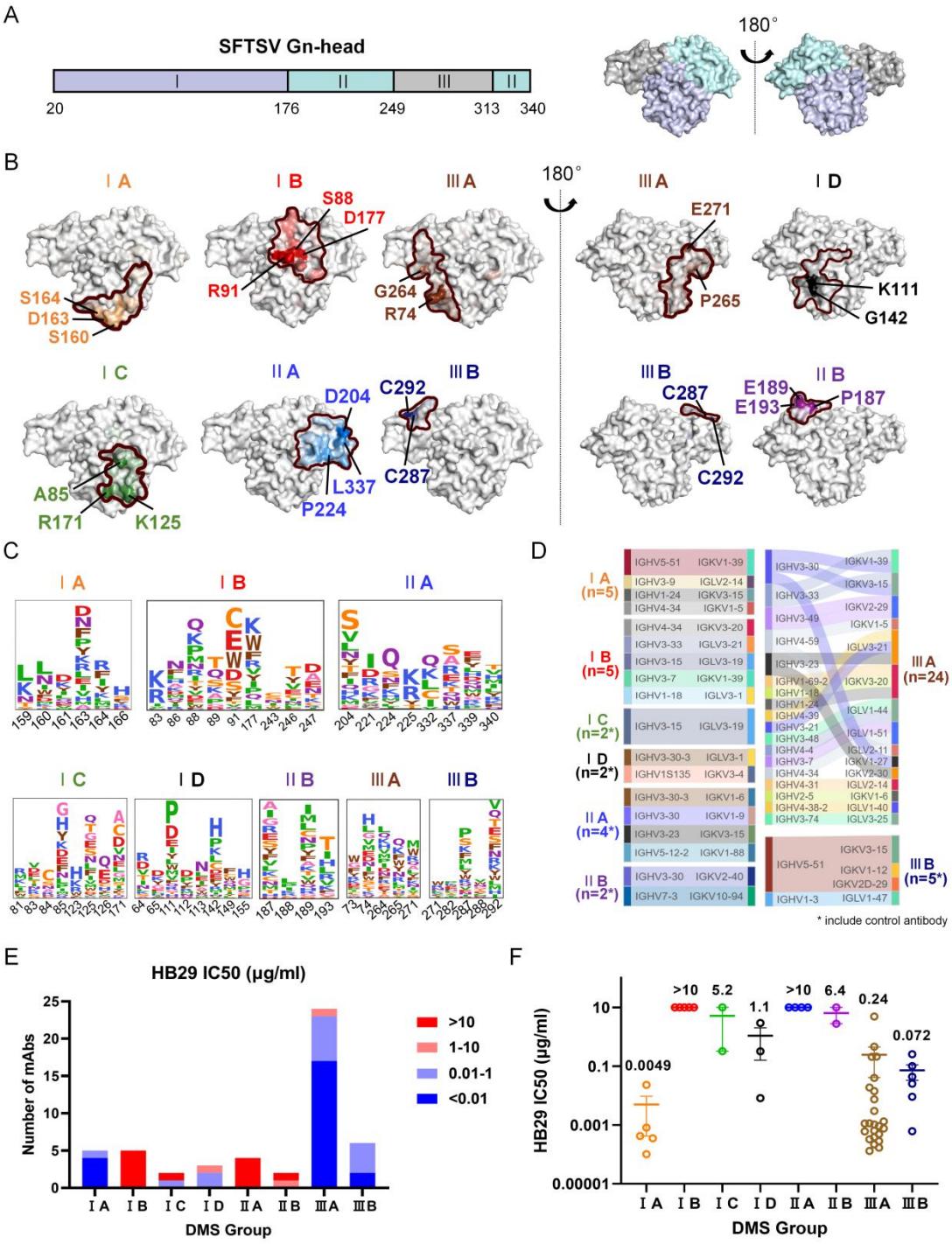

Fig. 2. Epitope analysis of all Gn antibodies by yeast DMS

(A) Structural schematic of SFTSV Gn-head. The left panel illustrates the delineation of the three domains, colored in blue-white (I), pale cyan (II), and gray (III), respectively; the corresponding structural schematic is shown in the right panel (PDB: 5Y10).

(B) Structural projections and key epitope annotations of the eight DMS groups with different colors. The region outlined by the curved line corresponds to the epitope of each respective group. In the structural projection, amino acid residues with higher DMS scores are displayed in darker colors.

(C) Average escape scores of antibodies in eight groups. Colors are assigned according to the type of amino acids, and the heights of the letters in the logo plot indicate escape scores. Residues are numbered based on Gn-head

bioRxiv preprint doi: https://doi.org/10.1101/2025.11.26.690690; this version posted November 30, 2025. The copyright holder for this preprint (which was not certified by peer review) is the author/funder, who has granted bioRxiv a license to display the preprint in perpetuity. It is made available under aCC-BY-NC 4.0 International license.

numbering.

(D) The gene analysis of the antibodies in eight groups. Sankey diagram was generated to visualize the correspondence between heavy and light chains for the antibody genes in each group, with asterisks indicating the inclusion of control antibodies.

(E-F) Statistical analysis of the number (E) and IC50 values (mean SEM) (F) for neutralization against the HB29 strain across DMS-classified antibody groups was performed.

bioRxiv preprint doi: https://doi.org/10.1101/2025.11.26.690690; this version posted November 30, 2025. The copyright holder for this preprint (which was not certified by peer review) is the author/funder, who has granted bioRxiv a license to display the preprint in perpetuity. It is made available under aCC-BY-NC 4.0 International license.

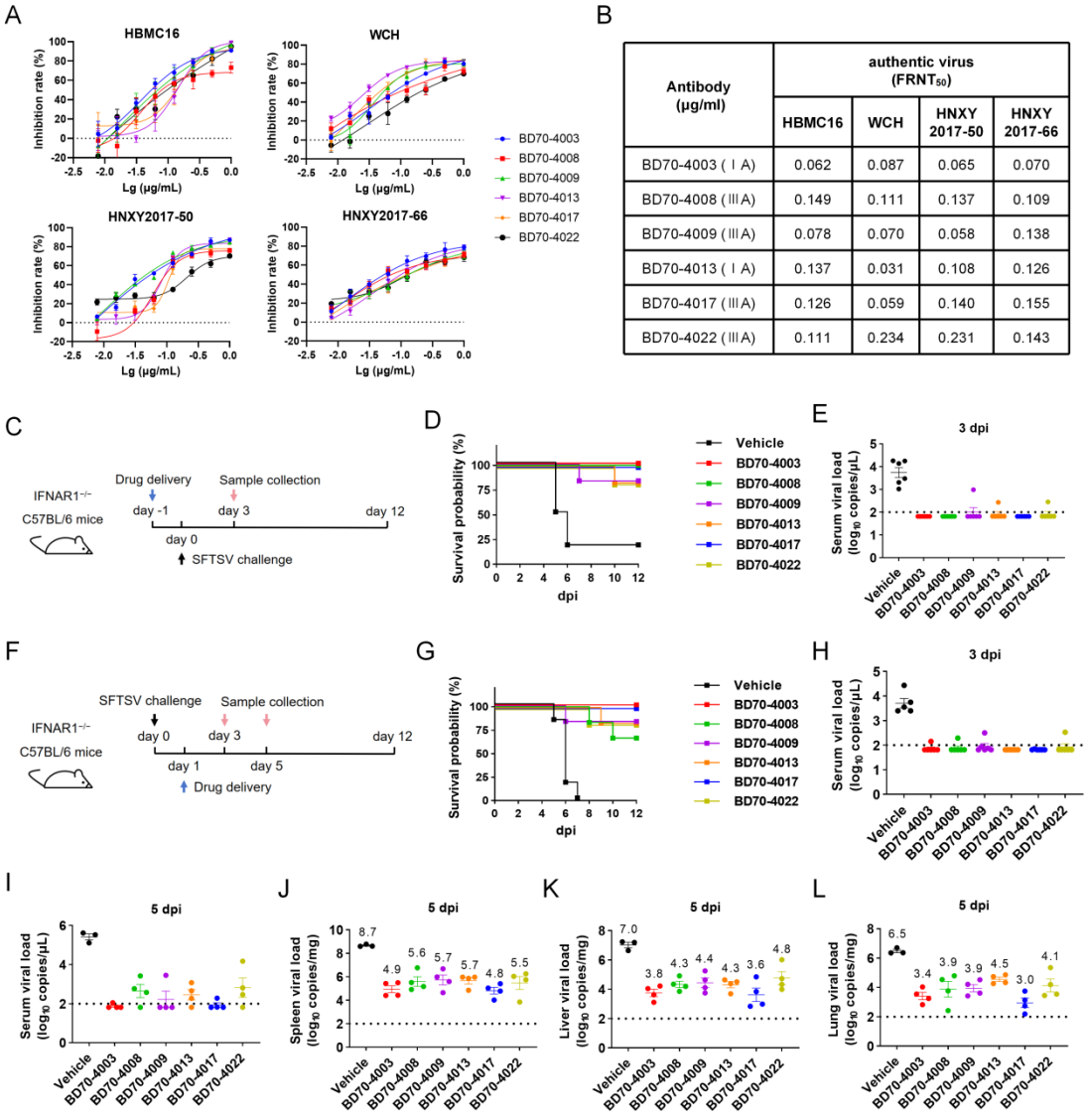

Antibody (μg/ml)	authentic virus (FRNT$_{50}$)			
	HBMC16	WCH	HNXY 2017-50	HNXY 2017-66
BD70-4003 (Ⅰ A)	0.062	0.087	0.065	0.070
BD70-4008 (Ⅲ A)	0.149	0.111	0.137	0.109
BD70-4009 (Ⅲ A)	0.078	0.070	0.058	0.138
BD70-4013 (Ⅰ A)	0.137	0.031	0.108	0.126
BD70-4017 (Ⅲ A)	0.126	0.059	0.140	0.155
BD70-4022 (Ⅲ A)	0.111	0.234	0.231	0.143

Fig. 3. MAb-mediated protection of authentic virus challenge *in vitro* and *in vivo*

(A-B) The neutralization activity of six selected mAbs against four SFTSV authentic virus. The $FRNT_{50}$ and IC_{80} were calculated using the equation of log [inhibitor] versus response-variable slope (four parameters) method. Data were shown as mean SD values from three biologically independent replicates.

(C and F) Schematic of the design for the HBMC16 challenge experiment in mice. In prophylactic groups (C), 5 mg/kg mAb was administered intraperitoneally and challenged by HBMC16 intraperitoneally 1 day later (C). In therapeutic groups (F), antibodies were given intraperitoneally 1 day after virus challenge. Each group consists of 6 mice.

(D and G) Survival curves of mice in each group.

(E and H-F) Viral load in the serum of mice in each group.

(J-L) Viral load (mean SD) of mice challenged by HBMC16 in spleen (J), liver (K), or lung (L). Each point corresponds to samples from a mouse. The limit of detection is about 1.81×10^2 copies/g and is shown as the dashed line.

bioRxiv preprint doi: https://doi.org/10.1101/2025.11.26.690690; this version posted November 30, 2025. The copyright holder for this preprint (which was not certified by peer review) is the author/funder, who has granted bioRxiv a license to display the preprint in perpetuity. It is made available under aCC-BY-NC 4.0 International license.

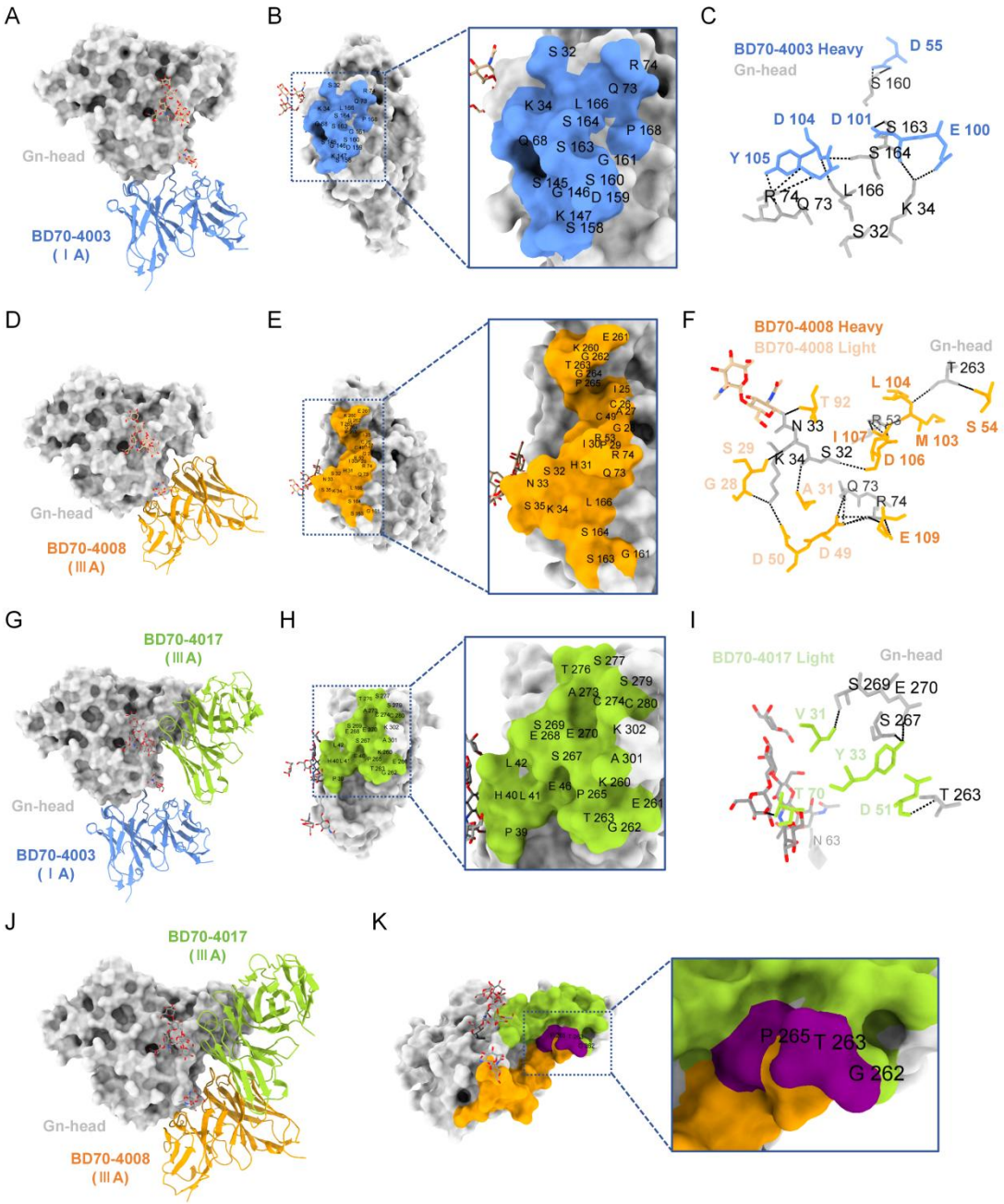

Fig. 4. Cryo-EM structure of Gn antibodies bound to HB29-Gn-head

(A, D, G and J) Aligned structures of BD70-4003 (A), BD70-4008 (D), BD70-4003/BD70-4017 (G) and BD70-4008/BD70-4017 (J) on SFTSV Gn-head. BD70-4003, BD70-4008 and BD70-4017 are colored in blue, orange, and green, respectively. Gn-head is colored in gray.

(B, E, and H) Surface representation of the contact residues on Gn-head interacting with BD70-4003 (B), BD70-4008 (E) and BD70-4017 (H).

(C, F, and I) Interactions between the heavy-chain and light-chain BD70-4003 (C), BD70-4008 (F) and BD70-4017 (I) and Gn-head. Residues of Gn-head, BD70-4003, BD70-4008 or BD70-4017 are gray, blue, orange, and green, respectively.

(K) The overlapping epitopes of BD70-4008 and BD70-4017 (K) are labeled in purple.

bioRxiv preprint doi: https://doi.org/10.1101/2025.11.26.690690; this version posted November 30, 2025. The copyright holder for this preprint (which was not certified by peer review) is the author/funder, who has granted bioRxiv a license to display the preprint in perpetuity. It is made available under aCC-BY-NC 4.0 International license.

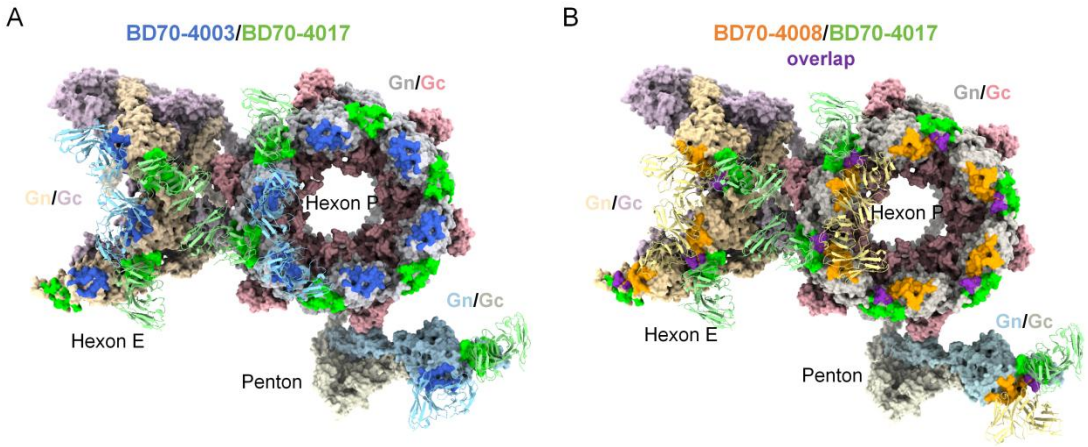

Fig. 5. Docking of three antibodies onto the surface of the SFTSV virion

Docking of BD70-4003/BD70-4017 (A) and BD70-4008/BD70-4017 (B) onto the surface of SFTSV virion (PDB: 8I4T). BD70-4003, BD70-4008 and BD70-4017 are colored in blue, orange, and green, respectively. The binding sites of mAbs on SFTSV virion are labeled with colors within the same palette.